Featured in Physics

Particle Sweeping and Collection by Active and Living Filaments

R. Sinaasappel,[1,*] K. R. Prathyusha,[2,*] H. Tuazon,[2] E. Mirzahossein,[1] P. Illien,[3] S. Bhamla,[2,†] and A. Deblais[1,‡]

[1]Van der Waals-Zeeman Institute, Institute of Physics, University of Amsterdam, 1098XH Amsterdam, The Netherlands

[2]School of Chemical and Biomolecular Engineering, Georgia Institute of Technology, Atlanta, Georgia 30332, USA

[3]Sorbonne Université, CNRS, Physicochimie des Electrolytes et Nanosystèmes Interfaciaux (PHENIX), Paris, France

(Received 13 June 2025; accepted 28 October 2025; published 5 January 2026)

Biological and robotic systems often operate in confined environments where materials must be gathered without centralized control. Inspired by the effective collection strategies of aquatic worms (*Lumbriculus variegatus* and *Tubifex tubifex*), we investigate how active filaments autonomously aggregate dispersed non-Brownian passive particles. We study this process across four platforms: living worms, a robotic chain, Brownian dynamics simulations of active polymers, and a coarse-grained toy model. We show that aggregation emerges from repeated contact and body deformation—effectively, a sweeping or brooming motion—and demonstrate that clustering dynamics are governed by filament length and bending stiffness. Across systems, particle gathering follows a shared aggregation-fragmentation process, where the steady-state cluster size approximately follows a quadratic increase with the effective width of the path cleared by the filament W relative to the domain size D. This scaling provides a minimal geometric baseline for comparison across active filamentous systems. We find that filament flexibility modulates W, enabling more flexible filaments to sweep larger areas and collect more particles. These results establish a unifying framework for understanding how shape and flexibility influence transport and organization in active filament systems and filamentous robots.

DOI: 10.1103/yxp1-t43g

Subject Areas: Biological Physics, Soft Matter

I. INTRODUCTION

Active, flexible filamentous materials are essential to a variety of biological and synthetic systems, where their capacity for self-organization, mechanical force generation, and adaptability drives critical functions such as locomotion, resource collection, and environmental restructuring [1,2]. Examples span from microscopic systems—motor-driven cytoskeletal filaments [3–8] and cilia [9,10]—to macroscopic organisms, including flagella [11–13], worms [1,14], and snakes [15]. Synthetic analogs such as self-propelled robots extend these concepts, utilizing flexibility and activity to adaptively explore their surroundings [16–18].

One striking manifestation of active material functionality is particle aggregation, a process observed in both natural and synthetic systems. For example, in freshwater ecosystems, oligochaetes like *Tubifex tubifex* and *Lumbriculus variegatus* (California blackworms) use coordinated motion and mucus secretions to aggregate dispersed particles [19–23], enabling nutrient cycling and habitat stabilization [24,25]. Similarly, robotic systems exploit activity and flexibility to manipulate inert (i.e., passive) materials, mimicking these natural behaviors to perform tasks like debris management and targeted delivery [18]. These aggregation dynamics are governed by the interplay between filament flexibility, activity, and the environmental context, yet the precise mechanisms remain elusive.

Beyond biological systems, active-passive mixtures provide a simplified yet insightful framework to explore aggregation phenomena from an active matter perspective. Active agents, such as bacteria, colloidal Janus particles, or robotic systems, impose stresses and collisions on passive components, giving rise to emergent behaviors like clustering [26], phase separation [27,28], and laning [29]. These processes may influence nutrient flows, structural formation, and ecosystem dynamics in natural habitats [30] while

*These authors contributed equally to this work.

†Contact author: saadb@chbe.gatech.edu

‡Contact author: a.deblais@uva.nl

inspiring novel applications in material assembly and robotics [18]. Notably, the role of filament flexibility in such mixtures remains underexplored [31,32], despite its relevance to both biological polymers [33] and synthetic systems [18,34].

In this study, we bridge the gap between biological and synthetic active systems by investigating the particle collection dynamics of slender and flexible *Tubifex tubifex* and *Lumbriculus variegatus* worms in a controlled environment. We quantify the impact of their conformation and dynamics on the aggregation of non-Brownian passive particles. Extending these insights, we construct larger-scale robotic filaments and perform simulations to examine how variations in filament flexibility and length influence performance across biological, robotic, and simulated systems. Our findings suggest that flexibility and activity are central to enhancing particle aggregation, offering a general framework for designing adaptable, soft robotic systems that can autonomously manipulate materials in constrained or complex environments.

II. COLLECTING EXPERIMENTS

The particle collection ability of the worms in confined environments presents both a biological puzzle and an exciting potential application for tasks such as microplastic collection, sorting, and cleaning [19]. To explore how this natural behavior can be generalized to active filaments, we investigate the collecting dynamics in three distinct active filament systems: two living, centimeter-scale biological worms, *T. tubifex* and *L. variegatus*, which differ in aspect ratio; a meter-scale robotic filament, designed to isolate the effects of filament parameters such as elasticity and length; and a Brownian dynamics simulation of an active filament with a tangentially propelling force [35–37] to validate and extend our experimental observations. Despite the fact that these two worms have similar appearances and quantitatively comparable collective behaviors [1,38], they exhibit distinct locomotion-diffusion-dominated random walks in *T. tubifex* and ballistic motion in *L. variegatus*, providing the opportunity to study and compare their mechanisms of dispersed passive particle collection [1].

A. Living biological filamentous worms

In our first quasi-2D experimental setup, we place a single *Tubifex tubifex* (with typical lengths $L_c = 25$–45 mm) or *Lumbriculus variegatus* ($L_c = 15$–35 mm) into a 35-mm-diameter (D) Petri dish filled with thermostated water ($T = 21\,°\mathrm{C}$) and N_t randomly dispersed sand particles (120 particles, $d_{p,\mathrm{sand}} = 0.7$ mm, total weight 50 mg, Supplemental Material, Fig. S1 [39]). The particles are light enough so that inertia does not influence their dynamics and large enough so that they are macroscopic and not subject to thermal fluctuations.

Once in the Petri dish, the worms, denser than water, crawl along the bottom via wriggling motion. Unlike algae or microplastics, which adhere to the worm's mucus [19], sand particles do not stick to the worm's body. Instead, the worm's self-propulsion displaces sand particles upon contact; otherwise, the particles remain stationary. This displacement occurs only through direct physical interactions, as the motion of the worm does not generate significant fluid flow in the medium. As the worm moves through the dish and reorients its direction at the boundaries, it actively gathers particles into progressively larger clusters over time, as shown in Fig. 1(a) (see Movie S1 [39] and Fig. S2 in the Supplemental Material [39]). Fluctuations arising from the worm's motion continuously fragment clusters, preventing unrestricted growth and maintaining a quasisteady state in which clusters form and break. This clustering behavior emerges from the interplay between the worm's flexibility and its dynamic adaptability, where the activity is distributed along an extended, flexible filament composed of many coupled active segments. This mechanism is distinct from the phase separation typically observed in dense active-passive mixtures [26,27], which generally requires a finite fraction of independent active particles to drive many-body demixing whereas, here, a single extended active filament with correlated dynamics is sufficient to generate large passive clusters.

To further analyze the clustering behavior and the role of filament flexibility, we use image analysis to track worm conformations and particle positions, allowing us to characterize the distribution of cluster sizes over time (see Sec. I and Fig. S3 of the Supplemental Material [39]). We define a group of n number particles as a cluster of size s_n (for simplicity, we refer to the cluster size as s unless otherwise specified), where each particle is within a distance of one particle size $d_{p,\mathrm{sand}}$ from at least one other particle in the group.

A typical result of the cluster size distribution at different times, $P(s)$, is shown in Fig. 1(a), right. As in previous studies looking at clustering in active systems [26,48,49], we find that a power law with an exponential cutoff, $P(s) = \mathcal{C} s^{-\gamma} \exp(-s/s^*)$, where $\mathcal{C}$ is the normalization constant ensuring $\sum_s P(s) = 1$, describes our data well. The fitted exponent γ increases over time (Table S2 in Ref. [39]), indicating reduced coarsening of the clusters.

Within a characteristic timescale of approximately 60 minutes, the cluster size distribution reaches a steady state. The average cluster size $\langle s \rangle = \sum s P(s)$ at long times is typically $\langle s \rangle_L \approx 10$ particles for both species of worms. Figure 1(a) shows results for one *T. tubifex* worm, but our results are comparable between worms. See Movie S1 in Ref. [39] for an example of the experiments and a comparison between the two studied worm species.

B. Active polymer simulation

We perform Brownian dynamics simulations using an active polymer model [35,36,50] (for details, see Sec. II in Ref. [39]), which has been shown to effectively capture the

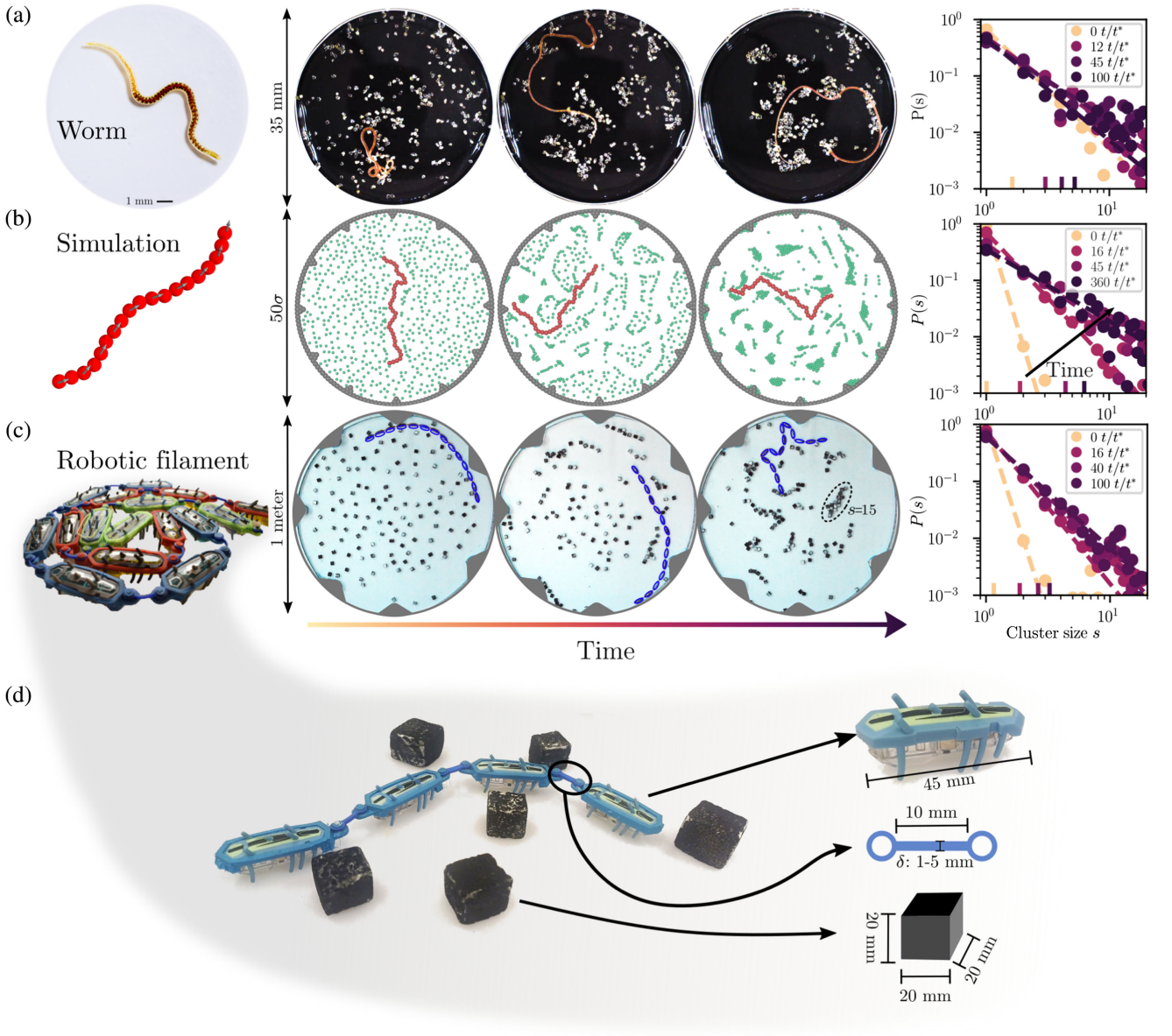

FIG. 1. Collection of passive particles by living, in silico, and robotic active filaments. (a) California blackworm (*Lumbriculus variegatus*) (left panel) and *T. tubifex* worm (right panels) in a Petri dish with sand particles. Over time, the worm gathers the sand into larger clusters, eventually reaching a steady state, as shown by the evolution of the cluster size distribution over time in the right panel. The mean value corresponding to the cluster size distribution is indicated on the x axis. Time is nondimensionalized by the characteristic time of one full passage of the filament's center of mass across the arena (t^*), allowing direct comparison across systems. (b) Active, tangentially driven filament interacting with non-Brownian passive particles exhibiting similar clustering behavior, where the cluster size distribution grows over time until reaching a steady state. The active force is applied to all monomers; for visual clarity, its direction is indicated by arrows on alternate monomers in the left panel. (c) Robotic filament composed of connected Hexbug robots moving within a circular arena, interacting with passive styrofoam cubes. The robotic filament collects particles into clusters, ultimately reaching a steady state. (d) Design details of the robotic filament and a close-up view of the styrofoam particles. The robotic units are connected via elastic rubber bands of tunable width δ, allowing control over the persistence length (ℓ_p) and contour length (ℓ_c) of the filament.

behavior of these worms [51]. Each monomer of size σ in the polymer follows overdamped Langevin dynamics, driven by an active force of amplitude f^a (the magnitude is 1) applied tangentially along the filament backbone. The flexibility of the active polymer is controlled by the bending stiffness κ between neighboring bonds [Fig. 1(b)]. In addition to the polymer length, the key parameters in our model are therefore reduced to f^a and κ.

In analogy with the living systems, we consider passive particles to be non-Brownian. These particles, with diameter

$d_{p,\mathrm{sim}} = 0.5\sigma$, are initially placed at a uniform concentration throughout the simulation domain. As observed in the worm experiments, there is no adhesion between the particles and the worms, nor any fluid flow generated by the worm motion, indicating that interactions are limited to short-range steric repulsion. In the simulation, the passive particles remain immobile until pushed by an active polymer segment, and they interact repulsively with other particles within a cutoff distance. The system thus represents a dry active environment, where the medium contributes only through single-particle friction (γ), and hydrodynamic interactions are neglected. We also perform additional simulations exploring more general scenarios, where particles exhibit attractive interactions or undergo random motion. Outcomes of the extended cases are compared in the discussion section, and details are provided in Secs. 2.D and 2.E of the Supplemental Material [39].

The time unit of the simulations is set by $\tilde{\tau} = \sigma^2\gamma/(k_BT)$. We systematically vary the number of monomers $N = 9$, 18, 28, 37, the number of passive particles $N_t = 50$, 100, 250, 500, 600, and the magnitude of bending stiffness κ in the range 0.01–10 to explore different filament flexibilities. These variations allow us to cover a broad range of contour lengths, particle densities, and filament flexibilities.

To ensure realistic boundary conditions, we place stationary particles along the circumference of a circular boundary of diameter $D = 50\sigma$. These boundary particles impart a steric repulsion to the active polymer and passive particles. Additionally, three-bead triangular "re-injectors" are positioned along the circular boundary at regular angular intervals $\theta = 30°$, with their apexes pointing toward the center of the confining circle (see Fig. S5 in Ref. [39]). This approach, commonly used in persistent active systems, prevents the filament from getting trapped along the walls [52,53]. When gliding near the wall, the tangentially driven filament is reoriented into the bulk of the arena by these triangular re-injectors, closely mimicking the behavior observed in biological worms (Supplemental Material, Fig. S2 [39]); different spacing of the re-injectors has no significant effect on the cluster formation (Supplemental Material, Fig. S5 [39]).

We find that the dynamics of the simulated active filament closely resemble those of the living worms, and the particles aggregate into clusters over time in a similar fashion [see the sequence of pictures in Fig. 1(b) and Movie S2 [39]]. This finding is confirmed by the cluster size distribution, which exhibits the same power-law behavior as in the worm experiments, with the distribution shifting toward larger values as time progresses [Fig. 1(b), right].

C. Robotic filament

In our second experimental setup, we scaled up the worm experimental platform to the meter scale and turned the worm into a robotic filament enclosed within a fixed arena of meter diameter [Fig. 1(c)]. Our active filament is composed of N commercially available self-propelled microbots (Hexbug Nano v2 with a characteristic size $\sigma_{\mathrm{unit}} = 45\,\mathrm{mm}$) [17,18,34,54,55], encased in a 3D-printed frame around each individual bot and elastically coupled by laser-cut silicone rubber connectors (Fig. 1(c); see also Supplemental Material Sec. III and Figs. S9 and S10 [39]). Adjusting the width of the connections [δ in the close-up of Fig. 1(c)], we can fine-tune the bending stiffness of the filament, κ.

We enclose the robotic filament using a rigid, circular metal boundary with a 120-cm diameter. To ensure consistency with our simulations, we incorporate re-injectors at the boundary to redirect the robotic filament into the bulk of the arena. The initially dispersed $N_t = 120$ passive cubic particles of size $d_{p,\mathrm{cube}} = 20$ mm, made of lightweight styrofoam, ensure that their weight does not play a role in the dynamics of the active robotic filament.

Interestingly, we observe that the robotic filament interacts with the particles in a manner similar to the biological and simulated systems, as confirmed by the probability distribution of cluster sizes over time [see Movie S3 [39] and Fig. 1(c), right]. This observation raises the question of why and how these active filaments, seemingly displaying universal behavior, manage to collect particles when confined in a circular arena. To address this issue, we next investigate the underlying factors that govern this particle collection process.

III. DYNAMICS OF AGGREGATION AND SPATIAL DISTRIBUTION

A. Aggregation-fragmentation dynamics and long-time average cluster size

To investigate the mechanisms driving particle clustering across our different active filament systems, we track the aggregation dynamics by measuring the average cluster size $\langle s \rangle$ over time. We also examine the influence of two key filament parameters: contour length (ℓ_c) and bending stiffness (κ) [Fig. 2(a)]. In our robotic system, the bending stiffness κ is controlled by adjusting the width of the elastic bonds (δ), with larger δ corresponding to increased stiffness. In simulations, in contrast, stiffness is controlled directly by tuning the bending potential parameter κ. In all systems, we measure the effective persistence length (ℓ_p) of the filaments by analyzing tangent-tangent correlations along the contour of the filament. In experiments, ℓ_p is extracted from image sequences, while in simulations, it is computed directly from the filament configuration data. This quantity correlates nontrivially with the initial bending stiffness κ [51], but it also captures changes in filament conformation due to activity and boundary interactions, where filaments tend to curl while following the arena edge. By normalizing the persistence length by the contour length of the filament (ℓ_p/ℓ_c), we obtain a common stiffness quantity that allows direct comparison between

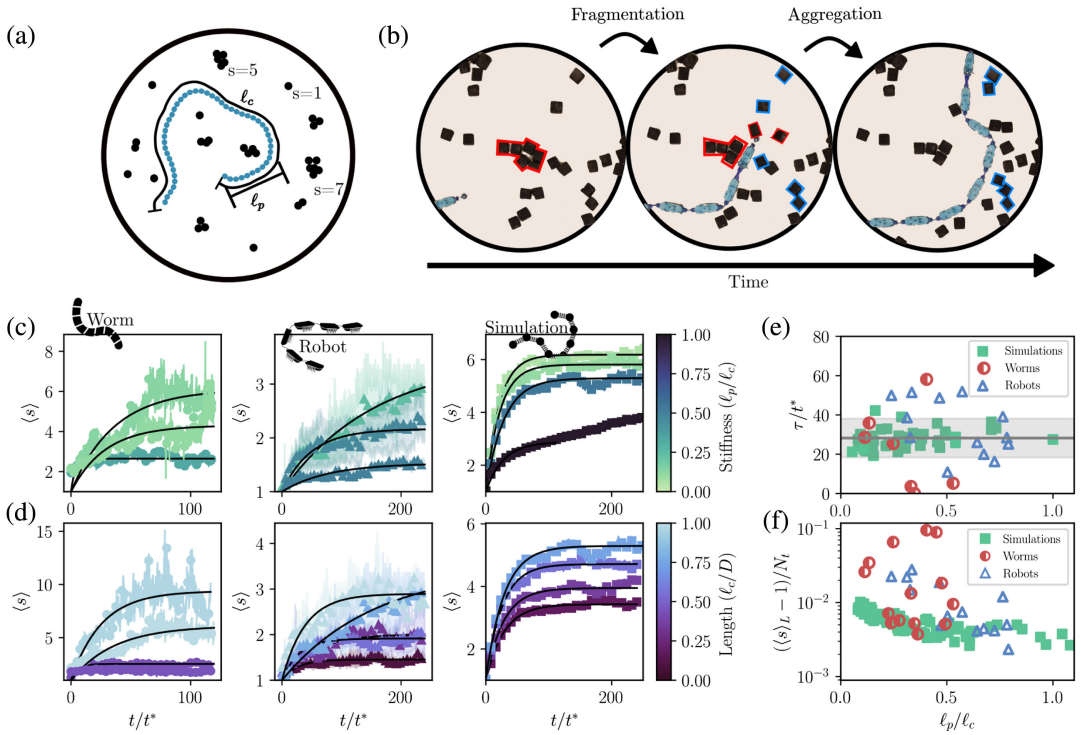

FIG. 2. Effect of filament length and flexibility on collecting dynamics and long-time average cluster size. (a) Active filamentous systems characterized by their flexibility (ℓ_p) and contour length (ℓ_c). The cluster size s is defined by the number of touching particles. (b) Larger cluster formation resulting from successive fragmentation (shown in red) and aggregation (shown in blue) processes, driven by interactions between the particles and the active filaments' conformations as they move through the arena. (c) Effect of the active filament's normalized stiffness (ℓ_p/ℓ_c) on the average cluster size. For all systems, the average cluster size grows over time before reaching a steady-state value $\langle s \rangle_L$ at long timescales, following Eq. (2). Lower filament stiffness leads to larger final cluster sizes. (d) Steady-state average cluster size increasing with the normalized filament length (ℓ_c/D) for fixed flexibility. (e),(f) Long-time steady-state cluster size $\langle s \rangle_L$ and characteristic aggregation timescale $\tau = k_{\text{eff}}^{-1}$, plotted as a function of filament stiffness (ℓ_p/ℓ_c). Values are obtained by fitting Eq. (2) to the data shown in panels (c) and (d). In panel (f), $\langle s \rangle_L$ is normalized by the total number of particles N_t to enable direct comparison across systems. The gray line in panel (e) shows the mean value across all data points ($n = 138$); shaded regions indicate standard deviation.

different systems, particularly useful for worms, whose bending stiffness cannot be controlled externally.

As shown in Fig. 1, all three systems exhibit strikingly similar behavior. When an active filament is introduced into an enclosed arena with randomly distributed particles, it sweeps particles along its path, driving both aggregation and fragmentation events [Fig. 2(b)]. This dynamic leads to the progressive formation of larger clusters, reminiscent of an aggregation-fragmentation process similar to polymerization reactions [56,57]. After a transient period, the system reaches a steady state where the average cluster size stabilizes, indicating that the aggregation and fragmentation rates have been balanced. In this analogy, the active filament acts as a dynamic reactor, driving both the aggregation and fragmentation of particle clusters.

From a theoretical perspective, the evolution of the system could, in principle, be treated as a binary process, where aggregation and fragmentation occur with rates k_a and k_f, which are typically functions of the sizes of the clusters m and m':

$$[s_m] + [s_{m'}] \underset{k_f(m,m')}{\overset{k_a(m,m')}{\rightleftharpoons}} [s_m + s_{m'}]. \tag{1}$$

The time evolution of the cluster size distribution is known to be sensitive to the functional dependence of k_a and k_f on the cluster sizes [56], which is generally difficult to measure accurately. Instead, we choose a simpler way and model the average cluster size $\langle s \rangle$ with a saturating exponential behavior:

$$\langle s(t) \rangle = 1 + \langle s \rangle_L (1 - e^{-k_{\text{eff}} t}), \tag{2}$$

which is compatible across all the systems we studied [Figs. 2(c) and 2(d)].

By fitting our data to Eq. (2), we extract both the long-term average cluster size $\langle s \rangle_L$ and the effective growth rate $k_{\text{eff}} = k_a + k_f$, determining the timescale for the system to reach the steady state. In particular, we find that this characteristic timescale τ is nearly independent of filament

length and stiffness across the different active filament systems studied here [Fig. 2(e)]. The system reaches a steady state after approximately $\tau/t^* \approx 30$ sweeps, where t^* is the typical time for a filament to cross straight (i.e., sweep) through the circular confinement (worms: $t^* \approx 120$ s; robots: $t^* \approx 5$ s; simulations: $t^* \approx 70\tilde{\tau}$). See Supplemental Material [39], Figs. S4 and S11, for an example of the determination of t^* [39]. It must be noted that defining t^* by a single value is an oversimplification since robots, and especially worms, follow trajectories more complex than repeated straight crossings (see Supplemental Material, Fig. S11 [39]). This simplification is likely the main cause of the large spread observed in τ.

Interestingly, both the flexibility and the contour length of the active filaments influence the final cluster size $\langle s \rangle_L$. As shown in Figs. 2(c) and 2(d), the filament stiffness (ℓ_p/ℓ_c) and the ratio of filament contour length to system size (ℓ_c/D) both affect the long-term cluster size: Longer and more flexible filaments tend to generate larger clusters.

While particle density and size also impact steady-state cluster sizes, we normalize these values by removing single-particle clusters and scaling by the total number of particles, defining ($\langle \tilde{s} \rangle_L = [(\langle s \rangle - 1)/(N_t)]$), to facilitate comparison across systems in the dilute limit (Supplemental Material, Fig. S6 [39]). Plotting this normalized long-time average cluster size allows us to compare biological, robotic, and simulated systems on equal footing. Figure 2(f) shows that the ratio ℓ_p/ℓ_c captures a general trend: More flexible active filaments (i.e., lower ℓ_p/ℓ_c) tend to form larger steady-state clusters. However, this trend does not yield a single collapsed curve across all systems, suggesting that an additional parameter governs clustering dynamics, which we explore in the next sections. Beyond characterizing the average cluster size, we also investigate how particles redistribute spatially within the arena as clustering evolves.

B. Spatial distribution

Figure 3(a) shows a typical sequence illustrating how clusters form preferentially near the arena center. To quantify this spatial distribution, we measure the mean radial position $\langle r \rangle$ of particles over time and compare it to the expected values for two limiting cases. In the case of full centralization, the mean radial position of particles is $\langle r \rangle \approx \frac{1}{3} d_p \sqrt{N_t}$ (with d_p the particle diameter), compared to $\langle r \rangle = \frac{2}{3} r_{\text{arena}}$ for an initially uniform distribution, which is highlighted by the gray line.

As shown in Fig. 3(b), long active filaments ($\ell_c/D \gtrsim 0.8$) tend to aggregate particles toward the center of the arena across all active filamentous systems studied. In contrast, shorter filaments ($\ell_c/D \lesssim 0.3$) tend to accumulate particles away from the center. In the limit of short filament length, this behavior resembles that of active pointlike particles in a bath of passive particles, which typically accumulate near boundaries or form a dispersed,

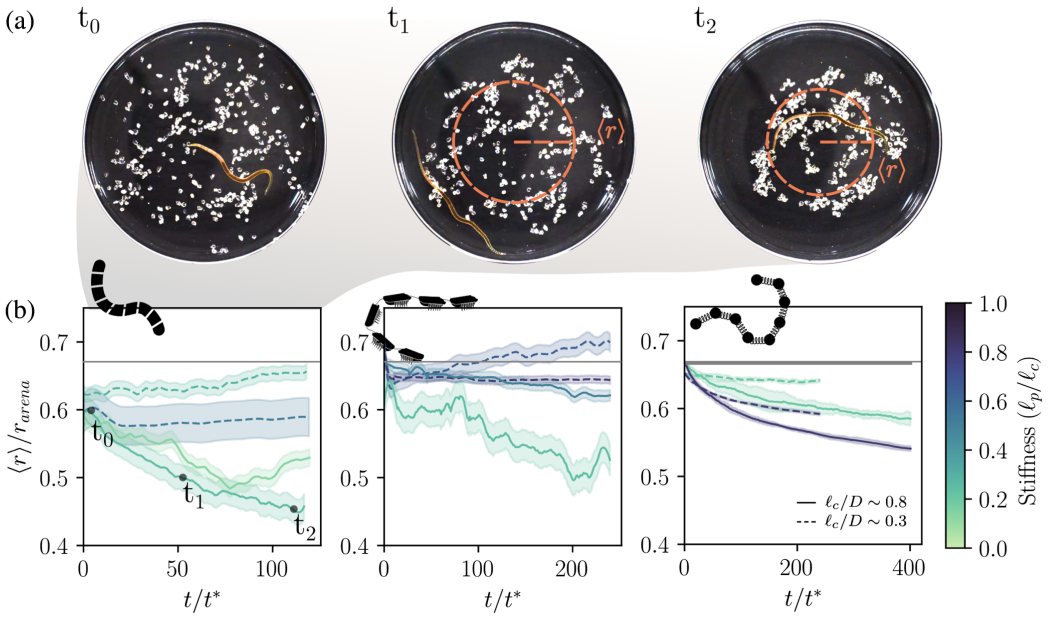

FIG. 3. Evolution of the cluster's average location over time. (a) Sequence of images ($t_i = t/t^* = 0$; 52; 120) showing the spatial evolution of particle positions over time. (b) Average radial position of the particles as a function of time for the three different active filamentous systems. Long filaments ($\ell_c/D \sim 1$) tend to accumulate particles at the center of the arena compared to short ones ($\ell_c/D \sim 0.3$), while stiffer filaments seem to be slightly more efficient at gathering particles to the center. Data shown for worms and robots are for representative single experiments, smoothed with a Savitzky-Golay filter. The shaded area indicates the magnitude of the noise. The horizontal line indicates the theoretical value for a uniform distribution in the arena, and the shaded area on the simulation data indicates the standard error.

gaslike state [34,58]. Stiffer filaments ($\ell_p/\ell_c \gtrsim 0.5$) appear more effective at centralizing clusters than flexible filaments of the same length, likely because more flexible filaments ($\ell_p/\ell_c \lesssim 0.3$) spend more time in the center of the arena, thereby pushing clusters outward (see Supplemental Material Fig. S10 for more details on typical trajectories of the filaments and Fig. S12 for snapshots of all experiments depicted in Fig. 3 [39]).

IV. ACTIVE SWEEPING COLLECTING MECHANISM

The striking similarities between the three filamentous systems suggest a general underlying physical process, which we aim to elucidate in this section. A detailed analysis of the conformation of active filaments during exploration reveals that they actively sweep particles away from their path as they move through the arena. As shown in the sequence of snapshots obtained from the simulation in Fig. 4(a), the trajectory of an active filament over time leaves behind a cleared path of effective width W. A probability density map of the filament's center-of-mass position over the entire course of its motion further reveals that the filaments spend a significant portion of their time near the boundary, effectively pushing particles away from it [Fig. 4(b)].

As mentioned before, despite the influence of filament length and flexibility on clustering [Fig. 2(f)], this relationship does not lead to a system-independent collapse across the different systems we studied here, which suggests that an additional parameter more directly controls the clustering dynamics.

We propose that the clustering process is better characterized by the effective width of the footprint, W, defined as the (average) transverse extent of the pathway cleared by the trajectory of the filament. As shown in Fig. 4(a), W depends on the filament's flexibility and length, with longer and more flexible filaments generally generating wider pathways. To quantify W, we first superimpose all consecutive contours of a filament in the period of time that the filament takes to cross the arena in order to find the footprint of the filament. Next, we fit the largest circle that can be inscribed inside this footprint and take the diameter of this circle to be the footprint width (Supplemental Material, Fig. S14 [39]). Systematic measurements (Supplemental Material, Fig. S15 [39]) confirm that more flexible filaments tend to exhibit larger transverse fluctuations relative to their tangential motion, leading to wider footprints. These fluctuations result from the complex conformation of the active polymer due to the interplay between filament activity, flexibility, and interactions

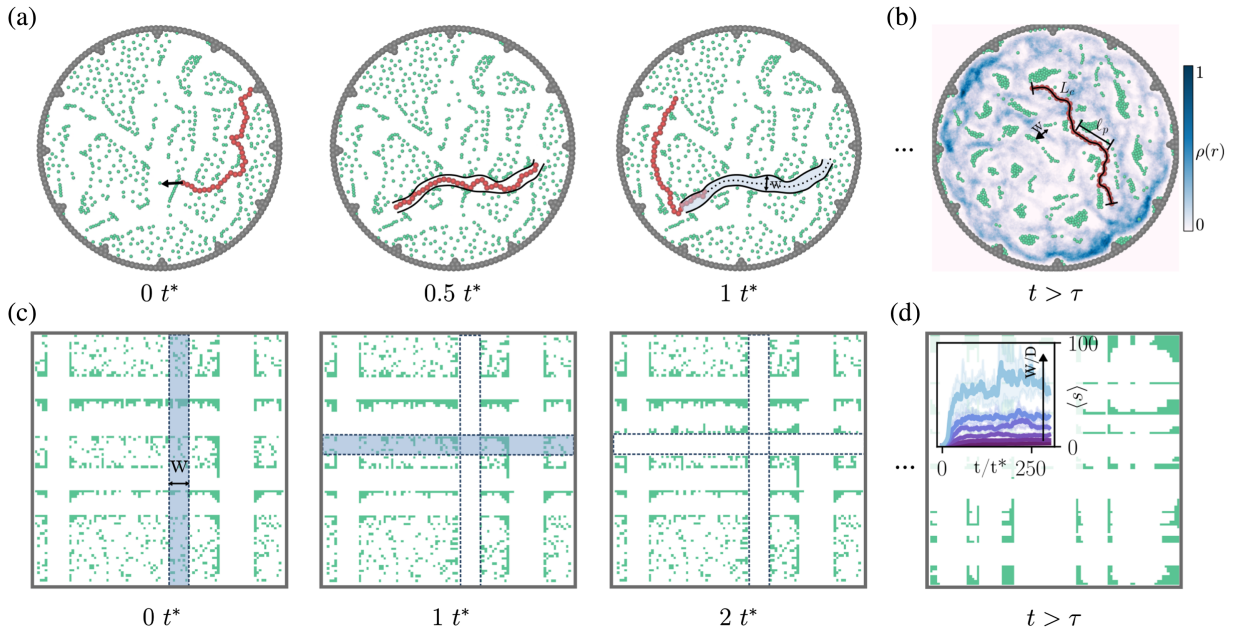

FIG. 4. Simplified "sweeping" model for particle aggregation dynamics. (a) Brownian dynamics simulation of an active filament ($\ell_p/\ell_c = 0.29$) sweeping through a field of particles, progressively clustering them into larger aggregates over time. (b) Heatmap of the filament's trajectory, showing the regions it has traversed [color bar indicates the probability density of the center of mass of the filament, $\rho(r)$]. As the filament moves, it clears particles along its path of width W, leaving unvisited areas where particles accumulate. (c) Particle displacement using a simplified system where bands of width W (representing the filament) sweep particles at each timestep within a confined arena. The sweeping bands are randomly placed and oriented either horizontally or vertically (see Supplemental Material, Sec. V [39]). (d) Steady-state cluster formation. The inset shows the evolution of the average cluster size over time, showing that this simplified model captures the aggregation dynamics observed in experiments and simulations [Figs. 2(c) and 2(d)] (see also Supplemental Material, Fig. S16 [39]).

with the arena boundaries. In particular, flexible simulated filaments with smaller ℓ_p display variable, curling trajectories that produce scattered values of W, whereas worms generate wider footprints because moderate flexibility enhances lateral excursions compared to both very stiff and very flexible limits. Filament length ℓ_c further modulates the footprint: Longer filaments sweep larger areas but also experience more self-interactions that reduce trajectory persistence. Finally, the confinement size D may constrain the range of accessible trajectories, such that larger arenas allow broader exploration and therefore relatively bigger footprint widths, while smaller ones limit both the effective W/D ratio and the characteristic timescale of final cluster formation.

When the final average cluster size $\langle s \rangle_L$ is plotted as a function of W, normalized by the system dimension D, all data from Fig. 2(f) collapse reasonably well onto a shared scaling curve, Fig. 5. This process establishes W as the key parameter governing the clustering process: The larger the effective footprint width, the larger the final average cluster size. Since W is set by filament flexibility and length, these properties indirectly dictate the clustering dynamics.

To understand the scaling behavior of $\langle s \rangle_L$ with W observed in Fig. 5, we propose a coarse-grained sweeping model (see Supplemental Material, Sec. V [39]). In this model, we start with a box of size $L \times L$ with N_t passive particles. Clustering occurs as particles are swept away from a region of size $L \times W$, representing the effective path cleared by the active filaments [see Fig. 4(c)]. Initially, the particles are uniformly distributed throughout the arena. Over time, repeated filament sweeps along both axes push particles away from these regions, leading to two competing effects: aggregation, where particles accumulate into larger clusters as they are displaced from swept regions, and

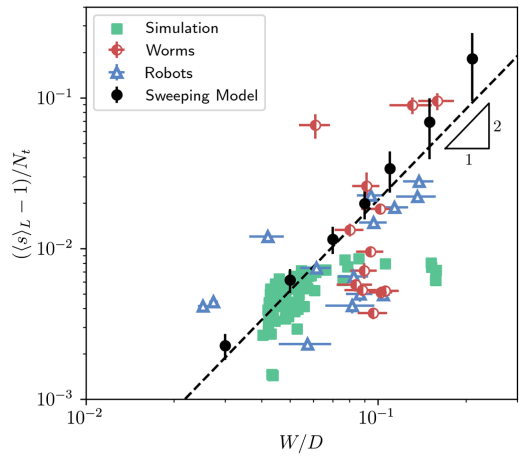

FIG. 5. Steady-state normalized cluster size as a function of filament footprint width. The long-time average cluster sizes from all experiments and simulations collapse onto a single master curve when plotted against the average active filament sweep width W. The dashed line shows the predicted scaling $\langle s \rangle_L \sim W^2$.

fragmentation, where clusters can be fragmented when the filament path crosses an aggregate (see Movie S4 [59]).

This minimal particle sweeping model quantitatively reproduces the experimentally observed clustering dynamics, as confirmed in the inset of Fig. 4(d), where the predicted cluster growth dynamics aligns with the experimental and simulation data of Figs. 2(c) and 2(d). Additionally, the timescale to reach a steady state also aligns very well with our experimental findings: After about 30 iterative sweeps, we converge to the steady state (see Supplemental Material, Sec. V and Fig. S16 for more details on the results of this model [39]).

Aggregation and fragmentation of particle clusters can generally be described by the Smoluchowski aggregation equation [40,56], which applies to irreversible aggregation and thus has inherent limitations in the context considered here (Supplemental Material, Sec. VI and Fig. S17 [39]). This theory relies on a mean-field approximation, assuming that each cluster interacts equally with all others, regardless of their relative separation. However, this assumption breaks down in our system, where the aggregation and fragmentation processes are governed by the motion of the active filament, which introduces spatial correlations and disrupts the equivalence between clusters. To account for these spatial effects, we propose a scaling relation using typical cluster separation and mass conservation.

Let a be the typical distance between two clusters and R the typical cluster size. If the cluster size distribution is sufficiently narrow, that is, the clusters are approximately the same size, the typical mass of a cluster M scales as R^2. Denoting by n_c the number density of clusters, mass conservation implies that $n_c M$ is constant and that $n_c \sim 1/R^2$. The distance between two clusters is typically $1/\sqrt{n_c}$, which yields $a \sim R$. In a steady state, the clusters remain unaffected by the sweep process when separated by a distance on the order of W, giving $a \sim W$. Combining these two conditions, we obtain $R \sim W$. Since the number of particles per cluster scales as R^2, this immediately leads to the scaling law $\langle s \rangle_L \sim W^2$, which rationalizes the experimental and simulation data collapse shown in Fig. 5.

As shown in Fig. 5, our sweeping model (black circles) and scaling argument (dashed line) predict that the long-time average cluster size scales as W^2, providing a minimal geometric baseline for comparison. This agreement between theory, simulations, and experiments highlights that the effective sweeping width W is a key parameter governing the clustering process. We also note that simulation results deviate from the predicted scaling at larger values of W, likely because our argument holds only when the sweep width remains small compared to the domain size, i.e., for $W/D \lesssim 1$. Even at moderate values, $W/D \sim 0.2$, deviations appear in simulations, whereas worms and robots generally follow the baseline trend. In this regime, active polymer simulations frequently adopt curling conformations [36], which reduce particle collection. Such conformations are less

prevalent in the experimental systems: Robots explore a broader range of normalized persistence lengths and exhibit systematic directional biases due to actuation, maintaining efficient sweeping; worms, while constrained to a narrower persistence length range, adapt their meandering, intermittent trajectories through biological sensing, avoiding trapped curled states and enhancing collection. These differences in conformational accessibility and trajectory control explain why worms and robots remain closer to the minimal geometric baseline than simulations in this domain.

Additionally, our sweeping model represents an idealized situation in which sweeping bands are randomly placed and oriented orthogonally across the domain, clearing particles in a simplified manner. In contrast, the worms, robotic filament, and tangentially driven filament sweep their surroundings via more complex trajectories, with finite-size effects associated with filament conformation, cluster size, and interactions with boundaries. These aspects warrant further detailed investigation.

V. DISCUSSION AND CONCLUDING REMARKS

A. Summary

Our work integrates biological experiments, robotic realizations, and computational modeling to uncover how flexible active filaments collect passive particles in confined environments. Through our investigation of *Tubifex tubifex* and *Lumbriculus variegatus* worms, as well as robotic analogs and simulations, we demonstrate that active filaments can autonomously cluster dispersed particles by dynamically sweeping (or brooming) across their surroundings. Our results highlight how filament flexibility, activity, and the dynamic footprint width W collectively govern the efficacy of particle aggregation, revealing a consistent scaling behavior. These findings not only highlight fundamental mechanisms underlying biological organization but also suggest design strategies for adaptable robotic systems and programmable active materials. It is therefore worthwhile to explore the broader implications of our study, particularly in the contexts of living systems, active-passive polymer mixtures, flexible active filament systems, and robotics, as discussed below.

B. Implications for living systems

Ecosystems continuously evolve through dynamic interactions between living organisms and their surrounding physical structures, as first illustrated by Darwin's seminal observations of earthworms gradually reshaping landscapes through sustained biological activity [60].

Across diverse ecosystems, the activity of animals, including trampling [61], grazing [62], and burrowing [63], can generate large-scale patterns, illustrating how biological interactions with the environment can give rise to ordered structures without centralized control [64]. Among aquatic ecosystems, similar spatial patterns emerge from the activity of benthic organisms that modify sediments through burrowing and feeding. For instance, aquatic worms such as *Tubifex tubifex* and *Lumbriculus variegatus* naturally engage in particle aggregation, influencing sediment structure, nutrient cycling, and oxygenation processes [20,65].

Previous studies have largely attributed this behavior in benthic macroinvertebrates to biological adhesion mechanisms, such as mucous secretions that facilitate the collection of organic and inorganic matter, including microplastics [19]. Our additional experiments and simulations, which introduce short-range attractive interactions between passive particles (Secs. 2.D and 3.C, Supplemental Material [39]), demonstrate that stronger attraction clearly promotes the formation of larger and more stable clusters compared to purely repulsive particles (Figs. S7 and S13, Supplemental Material [39]). Moreover, interactions with such stable clusters can induce conformational transitions in the active filament, from an extended to a rotating spiral-like state [Fig. S7(b), Supplemental Material [39]]. However, the results presented here indicate that the flexible body and active motion of worms alone are sufficient to reorganize their environment effectively, even in the absence of adhesion or long-range attractive interactions. Similar mechanisms are observed in other organisms, including marine polychaete worms [66], snakes [67], and nematodes (*C. elegans*) [68], which actively restructure granular or soft media through body undulations and locomotion. These findings suggest that the interplay between flexibility, activity, and physical interactions with the environment may represent a general principle for environmental reorganization, beyond species-specific adhesive mechanisms.

C. Implications for active-passive mixtures

From an active matter perspective, the results presented here offer new insights into the behavior of active-passive mixtures under confinement, where self-propelled agents navigate among passive, nonmotile components. In classical active matter systems, such mixtures often display clustering [26], phase separation [27,28], and pattern formation [29]. Here, we specifically examined a distinct regime in which activity is embedded within flexible chains and active filaments that interact mechanically with a collection of non-Brownian passive particles. This filamentous architecture introduces internal degrees of freedom such as bending and lateral fluctuations, which are absent in systems of pointlike or rigid active particles.

These transverse fluctuations play a central role in the reorganization of non-Brownian passive particles. The dynamic undulations of the filament laterally extend the effective swept area over time, continuously displacing and aggregating passive particles across the confined space. In the absence of adhesion, attractive interactions, passive particle motion, or external control, the filamental motion

alone is sufficient to generate emergent structures such as voids, clusters, and spatial heterogeneity in an otherwise dilute and disordered system. In real-world settings, environmental conditions such as flow or noise can lead to fluctuation of the passive particle motion, thus introducing a supplemental parameter in the aggregation process. In the presence of random noise, our simulations reveal that the average cluster size decreases with an increasing ratio of stochastic force strengths between passive beads and the filament, showing that stronger thermal noise suppresses cluster growth and stability (Fig. S8 in the Supplemental Material [39]). Here, further work could systematically investigate the effect of noise on the aggregation dynamics but also on the role of confinement, particle density, and propulsive force that may impact the dynamics of aggregation and the stability of the clusters.

This sweeping mechanism extends previous strategies that used rigid active colloids [69] or chiral bacterial baths [70] to control passive assembly. Our results demonstrate that flexibility enhances the capacity of active agents to manipulate their surroundings. This finding has implications for biological systems where active filaments must navigate and reorganize dense passive environments. In cells, for instance, cytoskeletal filaments such as actin and microtubules operate within crowded spaces filled with organelles and macromolecular assemblies. While motor-driven transport along filaments is well studied, the role of intrinsic filament motion in spatial reorganization remains poorly understood [71]. In addition, our work adds to the existing literature on active polymer research that has shown how the interplay between activity, flexibility, and propulsion mechanisms [72] can lead to conformational changes and facilitate exploration [73], contributing to dynamic organization in crowded [74] and complex environments [75–77], by revealing how these effects emerge under confinement and through interactions with passive particles.

By showing that activity and flexibility alone can drive large-scale restructuring, our findings suggest a mechanical route to organization in both biological and synthetic systems. More broadly, they highlight how flexible active filaments reshape active-passive interactions, offering principles for designing self-organizing materials that adapt to and reconfigure their environment.

D. Implications for soft robotics

Tubifex tubifex and *Lumbriculus variegatus* worms occupy a region of relatively large final average cluster size (Fig. 5), indicating that their particle aggregation strategies are mechanically well optimized. Our sweeping model predicts that active filaments with a larger effective footprint width W can form even larger clusters. Guided by this principle, we extended the approach to our robotic filaments. By tuning their flexibility, we effectively controlled their footprint width W, offering a direct strategy to influence the final cluster size. This mechanical adaptability highlights a simple design rule for improving the collecting performance of soft robotic filaments.

Additional strategies can be employed to enhance the collection efficacy of an active filament, as illustrated in Fig. 6 and Movie S5 [59]. One approach involves modifying the filament topology by introducing branching structures, which increases the overall footprint of the active filament [Fig. 6(b)]. Another approach consists of tuning the self-propulsion velocity along the filament, which can be achieved by locally varying the activity of the bots or, in our case, by changing the weight distribution of the leading bots. This approach induces dynamic oscillations of the filament, resembling flagellar beating or snakelike motion, which effectively increases its footprint width as it moves through the arena [Fig. 6(c)]. Finally, tuning the bending stiffness of the filament to impose a local curvature allows particles to be scooped along the path of the active filament [Fig. 6(d)].

All of these strategies can be understood as ways of modifying the effective sweep width W of the robotic filament. By increasing or redistributing W, the filament explores a larger area and thereby collects more particles, leading to an increase in the long-time average cluster size $\langle s \rangle_L$ compared to a simple linear chain [Fig. 6(e)]. However, the design space introduced here does not provide direct control over the number of clusters: Repulsive particles still organize into several coexisting aggregates, i.e., a form of microphase separation. This outcome mirrors the biological scenario observed in worms but also highlights that achieving single-cluster collection remains an open challenge. Our goal here is not to optimize filament geometry but to demonstrate that W is a tunable design parameter. Future robotic designs could systematically vary branching, propulsion asymmetry, or curvature to maximize W and achieve more targeted control. Figure 6 should therefore be viewed as a proof of principle that filament geometry can bias clustering outcomes through systematic variation of W, providing a first step toward rational design of shape-adaptable soft robots for targeted collection tasks.

We also note that there are limits to this design space. When the filament becomes too wide, for instance, by adding branches to the front or by increasing the size of its monomers, it can become irreversibly stuck at the boundaries [see inset of Fig. 6(b)]. This limitation points to another way in which worms appear to be well adapted to their environment. The footprint width of a worm is not fixed but adjusts dynamically through transverse fluctuations. This polymer-like flexibility allows the worm to remain narrow in confined regions and broaden when space permits, enabling effective exploration and collection.

The strategies that we propose here open several directions for future work and extend recent studies showing how geometry and internal activity can enable soft robotic materials to perform tasks without the need for external

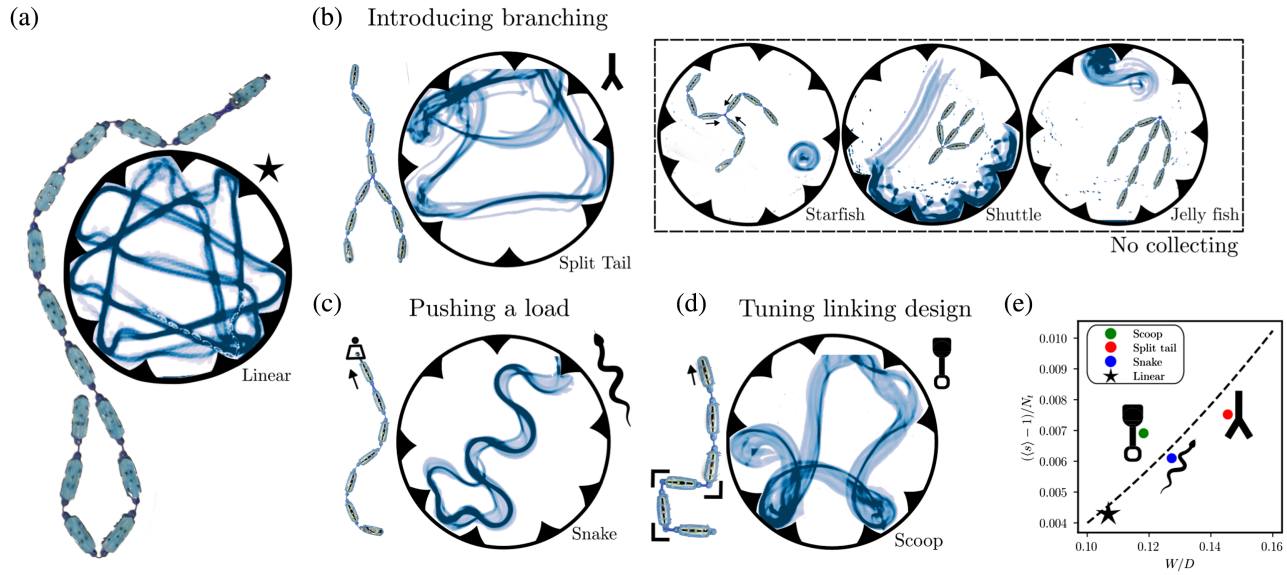

FIG. 6. Active filament atlas: design strategies for particle "brooming" and collection. (a) Baseline linear polymer configuration. The dark blue trails represent the trajectory of the robot over time, indicating the area explored. (b) First strategy, which modifies the chain topology by introducing branches, altering sweeping dynamics. Trajectories of each robotic unit within the chain illustrate distinct collection strategies. The split-tail design increases the effective footprint via a rear branch. The inset shows other branched configurations (starfish, shuttle, jellyfish) that exhibit disorganized or rotational motion and fail to collect particles effectively. (c) Second strategy, which adjusts the speed of the leading bot by increasing its weight, inducing self-oscillatory motion along the path. This snake configuration dynamically broadens the swept area, as reflected in the curved trajectories. (d) Tuning the elasticity of individual bonds enables the imposition of complex, preprogrammed curvatures during motion. This scoop configuration uses its intrinsic shape to steer particles along the inner arc as it moves through the arena. (e) Comparison of the resulting collection efficacy, quantified by the long-time average cluster size $\langle s \rangle_L$. This case demonstrates that geometry can bias clustering outcomes: While the linear chain (star symbol) produces small clusters, alternative designs achieve larger aggregates by sweeping particles more effectively, which illustrates proof-of-principle design strategies, showing that filament shape provides a tunable parameter to modulate clustering behavior. This finding establishes a first taxonomy of robotic active filaments, highlighting that geometry, not only activity, can be exploited as a control knob for programmable particle collection.

control or feedback [18,78,79]. While our results show that active filaments hold promise for simple environmental manipulations, achieving reliable and targeted control remains a key challenge. For instance, guiding the transport of passive particles requires control over the filament's trajectory. Strategies such as creating predefined pathways for filament motion or using controlled stimuli, such as light, to locally actuate the filament represent promising, yet largely unexplored, solutions.

ACKNOWLEDGMENTS

We thank the Technology Center of the University of Amsterdam for technical support and assistance with the tracking-based machine learning. All simulations were performed using resources provided by the Partnership for an Advanced Computing Environment (PACE) at the Georgia Institute of Technology, USA. We also thank Nico Schramma and Mazi Jalaal for fruitful discussions, and Ishant Tiwari for critical reading of the manuscript. S. B. acknowledges funding support from National Institutes of Health Grant No. R35GM142588, National Science Foundation (NSF) Grant No. PHY-2310691, NSF CAREER iOS-1941933, and Schmidt Sciences, LLC.

DATA AVAILABILITY

All data depicted in the figures of this text can be found in Ref. [59]. Raw data and computational models are available upon request.

[1] A. Deblais, K. R. Prathyusha, R. Sinaasappel, H. Tuazon, I. Tiwari, V. P. Patil, and M. S. Bhamla, *Worm blobs as entangled living polymers: From topological active matter to flexible soft robot collectives*, Soft Matter **19**, 7057 (2023).

[2] R. G. Winkler and G. Gompper, *The physics of active polymers and filaments*, J. Chem. Phys. **153** (2020).

[3] S. Ganguly, L. S. Williams, I. M. Palacios, and R. E. Goldstein, *Cytoplasmic streaming in Drosophila oocytes varies with kinesin activity and correlates with the microtubule cytoskeleton architecture*, Proc. Natl. Acad. Sci. U.S.A. **109**, 15109 (2012).

[4] F. Nédélec, T. Surrey, A. C. Maggs, and S. Leibler, *Self-organization of microtubules and motors*, Nature (London) **389**, 305 (1997).

[5] Y. Sumino, K. H. Nagai, Y. Shitaka, D. Tanaka, K. Yoshikawa, H. Chaté, and K. Oiwa, *Large-scale vortex lattice emerging from collectively moving microtubules*, Nature (London) **483**, 448 (2012).

[6] L. Le Goff, F. Amblard, and E. M. Furs, *Motor-driven dynamics in actin-myosin networks*, Phys. Rev. Lett. **88**, 018101 (2001).

[7] T. Sanchez, D. T. Chen, S. J. DeCamp, M. Heymann, and Z. Dogic, *Spontaneous motion in hierarchically assembled active matter*, Nature (London) **491**, 431 (2012).

[8] I. Kirchenbuechler, D. Guu, N. A. Kurniawan, G. H. Koenderink, and M. P. Lettinga, *Direct visualization of flow-induced conformational transitions of single actin filaments in entangled solutions*, Nat. Commun. **5**, 5060 (2014).

[9] M. A. Sleigh, *The Biology of Cilia and Flagella* (Macmillan, New York, 1962).

[10] A. S. Shah, Y. Ben-Shahar, T. O. Moninger, J. N. Kline, and M. J. Welsh, *Motile cilia of human airway epithelia are chemosensory*, Science **325**, 1131 (2009).

[11] S. L. Bardy, S. Y. Ng, and K. F. Jarrell, *Prokaryotic motility structures*, Microbiology **149**, 295 (2003).

[12] C. I. Mayfield and W. E. Inniss, *A rapid, simple method for staining bacterial flagella*, Can. J. Microbiol. **23**, 1311 (1977).

[13] B. M. Friedrich, I. H. Riedel-Kruse, J. Howard, and F. Jülicher, *High-precision tracking of sperm swimming fine structure provides strong test of resistive force theory*, J. Exp. Biol. **213**, 1226 (2010).

[14] V. P. Patil, H. Tuazon, E. Kaufman, T. Chakrabortty, D. Qin, J. Dunkel, and M. S. Bhamla, *Ultrafast reversible self-assembly of living tangled matter*, Science **380**, 392 (2023).

[15] J. Gray, *The mechanism of locomotion in snakes*, J. Exp. Biol. **23**, 101 (1946).

[16] C. Hernández-López, P. Baconnier, C. Coulais, O. Dauchot, and G. Düring, *Model of active solids: Rigid body motion and shape-changing mechanisms*, Phys. Rev. Lett. **132**, 238303 (2024).

[17] E. Zheng, M. Brandenbourger, L. Robinet, P. Schall, E. Lerner, and C. Coulais, *Self-oscillation and synchronization transitions in elastoactive structures*, Phys. Rev. Lett. **130**, 178202 (2023).

[18] Y. Xi, T. Marzin, R. B. Huang, T. J. Jones, and P.-T. Brun, *Emergent behaviors of buckling-driven elasto-active structures*, Proc. Natl. Acad. Sci. U.S.A. **121**, e2410654121 (2024).

[19] H. Tuazon, C. Nguyen, E. Kaufman, I. Tiwari, J. Bermudez, D. Chudasama, O. Peleg, and M. Bhamla, *Collecting–gathering biophysics of the blackworm lumbriculus variegatus*, Integr. Comp. Biol. **63**, 1474 (2023).

[20] K. W. Cummins and M. J. Klug, *Feeding ecology of stream invertebrates*, Annu. Rev. Ecol. Evol. Syst. **10**, 147 (1979).

[21] B. P. Ilyashuk, *Littoral oligochaete (annelida: Oligochaeta) communities in neutral and acidic lakes in the Republic of Karelia, Russia*, Boreal Env. Res. **4**, 277 (1999).

[22] D. G. Cook, *Observations on the life history and ecology of some lumbriculidae (annelida, oligochaeta)*, Hydrobiologia **34**, 561 (1969).

[23] R. S. Wotton, *The Biology of Particles in Aquatic Systems* (CRC Press, Boca Raton, 1994).

[24] E. Kristensen, G. Penha-Lopes, M. Delefosse, T. Valdemarsen, C. O. Quintana, and G. T. Banta, *What is bioturbation? The need for a precise definition for fauna in aquatic sciences*, Mar. Ecol. Prog. Ser. **446**, 285 (2012).

[25] K. R. Roche, A. F. Aubeneau, M. Xie, T. Aquino, D. Bolster, and A. I. Packman, *An integrated experimental and modeling approach to predict sediment mixing from benthic burrowing behavior*, Environ. Sci. Technol. **50**, 10047 (2016).

[26] S. Gokhale, J. Li, A. Solon, J. Gore, and N. Fakhri, *Dynamic clustering of passive colloids in dense suspensions of motile bacteria*, Phys. Rev. E **105**, 054605 (2022).

[27] P. Dolai, A. Simha, and S. Mishra, *Phase separation in binary mixtures of active and passive particles*, Soft Matter **14**, 6137 (2018).

[28] J. Stenhammar, R. Wittkowski, D. Marenduzzo, and M. E. Cates, *Activity-induced phase separation and self-assembly in mixtures of active and passive particles*, Phys. Rev. Lett. **114**, 018301 (2015).

[29] S. R. McCandlish, A. Baskaran, and M. F. Hagan, *Spontaneous segregation of self-propelled particles with different motilities*, Soft Matter **8**, 2527 (2012).

[30] A. W. Visser, *Biomixing of the oceans?*, Science **316**, 838 (2007).

[31] K. R. Prathyusha, *Passive particle transport using a transversely propelling polymer "sweeper"*, Soft Matter **19**, 4001 (2023).

[32] B. Zhang, T. Lei, and N. Zhao, *Comparative study of polymer looping kinetics in passive and active environments*, Phys. Chem. Chem. Phys. **23**, 12171 (2021).

[33] J. Smrek and K. Kremer, *Small activity differences drive phase separation in active-passive polymer mixtures*, Phys. Rev. Lett. **118**, 098002 (2017).

[34] A. Deblais, T. Barois, T. Guerin, P.-H. Delville, R. Vaudaine, J. S. Lintuvuori, J.-F. Boudet, J.-C. Baret, and H. Kellay, *Boundaries control collective dynamics of inertial self-propelled robots*, Phys. Rev. Lett. **120**, 188002 (2018).

[35] K. R. Prathyusha, S. Henkes, and R. Sknepnek, *Dynamically generated patterns in dense suspensions of active filaments*, Phys. Rev. E **97**, 022606 (2018).

[36] R. E. Isele-Holder, J. Elgeti, and G. Gompper, *Self-propelled worm-like filaments: Spontaneous spiral formation, structure, and dynamics*, Soft Matter **11**, 7181 (2015).

[37] M. Fazelzadeh, Q. Di, E. Irani, Z. Mokhtari, and S. Jabbari-Farouji, *Active motion of tangentially driven polymers in periodic array of obstacles*, J. Chem. Phys. **159**, 224903 (2023).

[38] Y. Ozkan-Aydin, D. I. Goldman, and M. S. Bhamla, *Collective dynamics in entangled worm and robot blobs*, Proc. Natl. Acad. Sci. U.S.A. **118**, e2010542118 (2021).

[39] See Supplemental Material at http://link.aps.org/supplemental/10.1103/yxp1-t43g for more details on the

experimental methods, setup, simulations, and Supplemental Videos. It includes Refs. [1,17,19,40–47].

[40] V. Smoluchowski and I. D. im unbegrenzten Raum, *Zusammenfassende bearbeitungen*, Ann. Phys. (N.Y.) **21**, 756 (1906).

[41] A. Deblais, S. Woutersen, and D. Bonn, *Rheology of entangled active polymer-like T. Tubifex worms*, Phys. Rev. Lett. **124**, 188002 (2020).

[42] A. Deblais, A. C. Maggs, D. Bonn, and S. Woutersen, *Phase separation by entanglement of active polymerlike worms*, Phys. Rev. Lett. **124**, 208006 (2020).

[43] T. Heeremans, A. Deblais, D. Bonn, and S. Woutersen, *Chromatographic separation of active polymer like worm mixtures by contour length and activity*, Sci. Adv. **8**, eabj7918 (2022).

[44] H. Tuazon, E. Kaufman, D. I. Goldman, and M. Bhamla, *Oxygenation-controlled collective dynamics in aquatic worm blobs*, Integr. Comp. Biol. **62**, 890 (2022).

[45] H. Tuazon, S. David, K. Ma, and S. Bhamla, *Leeches predate on fast-escaping and entangling blackworms by spiral entombment*, Integr. Comp. Biol. **64**, 1408 (2024).

[46] J. D. Weeks, D. Chandler, and H. C. Andersen, *Role of repulsive forces in determining the equilibrium structure of simple liquids*, J. Chem. Phys. **54**, 5237 (1971).

[47] K. Kremer and G. S. Grest, *Dynamics of entangled linear polymer melts: A molecular-dynamics simulation*, J. Chem. Phys. **92**, 5057 (1990).

[48] F. Ginot, I. Theurkauff, F. Detcheverry, C. Ybert, and C. Cottin-Bizonne, *Aggregation-fragmentation and individual dynamics of active clusters*, Nat. Commun. **9**, 696 (2018).

[49] G. S. Redner, C. G. Wagner, A. Baskaran, and M. F. Hagan, *Classical nucleation theory description of active colloid assembly*, Phys. Rev. Lett. **117**, 148002 (2016).

[50] J. Martín-Roca, E. Locatelli, V. Bianco, P. Malgaretti, and C. Valeriani, *Tangentially active polymers in cylindrical channels*, SciPost Phys. **17**, 107 (2024).

[51] R. Sinaasappel, M. Fazelzadeh, T. Hooijschuur, Q. Di, S. Jabbari-Farouji, and A. Deblais, *Locomotion of active polymerlike worms in porous media*, Phys. Rev. Lett. **134**, 128303 (2025).

[52] J. Deseigne, O. Dauchot, and H. Chaté, *Collective motion of vibrated polar disks*, Phys. Rev. Lett. **105**, 098001 (2010).

[53] J. Deseigne, S. Léonard, O. Dauchot, and H. Chaté, *Vibrated polar disks: Spontaneous motion, binary collisions, and collective dynamics*, Soft Matter **8**, 5629 (2012).

[54] G. A. Patterson, P. I. Fierens, F. Sangiuliano Jimka, P. G. König, Á. Garcimartín, I. Zuriguel, L. A. Pugnaloni, and D. R. Parisi, *Clogging transition of vibration-driven vehicles passing through constrictions*, Phys. Rev. Lett. **119**, 248301 (2017).

[55] O. Dauchot and V. Démery, *Dynamics of a self-propelled particle in a harmonic trap*, Phys. Rev. Lett. **122**, 068002 (2019).

[56] P. L. Krapivsky, S. Redner, and E. Ben-Naim, *A Kinetic View of Statistical Physics* (Cambridge University Press, Cambridge, England, 2010).

[57] R. M. Ziff, *Kinetics of polymerization*, J. Stat. Phys. **23**, 241 (1980).

[58] J. Bouvard, F. Moisy, and H. Auradou, *Ostwald-like ripening in the two-dimensional clustering of passive particles induced by swimming bacteria*, Phys. Rev. E **107**, 044607 (2023).

[59] https://github.com/deb-lab/Supplementary-Movies-collecting.

[60] C. Darwin, *The Formation of Vegetable Mould through the Action of Worms* (D. Appleton, London, 1898), Vol. 16.

[61] B. Seleb, A. Chatterjee, and S. Bhamla, *Moving mountains: Grazing agents drive terracette formation on steep hillslopes*, arXiv:2504.17496.

[62] J.-C. Menaut and B. Walker, *Banded Vegetation Patterning in Arid and Semiarid Environments: Ecological Processes and Consequences for Management* (Springer Science & Business Media, New York, 2001), Vol. 149.

[63] M. Louw, P. Le Roux, E. Meyer-Milne, and N. Haussmann, *Mammal burrowing in discrete landscape patches further increases soil and vegetation heterogeneity in an arid environment*, J. Arid Environ. **141**, 68 (2017).

[64] R. M. Pringle and C. E. Tarnita, *Spatial self-organization of ecosystems: Integrating multiple mechanisms of regular-pattern formation*, Annu. Rev. Entomol. **62**, 359 (2017).

[65] A. Kudrolli and B. Ramirez, *Burrowing dynamics of aquatic worms in soft sediments*, Proc. Natl. Acad. Sci. U.S.A. **116**, 25569 (2019).

[66] S. Grill and K. M. Dorgan, *Burrowing by small polychaetes–mechanics, behavior and muscle structure of capitella sp.*, J. Exp. Biol. **218**, 1527 (2015).

[67] H. Marvi, C. Gong, N. Gravish, H. Astley, M. Travers, R. L. Hatton, J. R. Mendelson III, H. Choset, D. L. Hu, and D. I. Goldman, *Sidewinding with minimal slip: Snake and robot ascent of sandy slopes*, Science **346**, 224 (2014).

[68] G. Juarez, K. Lu, J. Sznitman, and P. E. Arratia, *Motility of small nematodes in wet granular media*, Euro. Phys. Lett. **92**, 44002 (2010).

[69] M. C. Pedersen, S. Mukherjee, A. Doostmohammadi, C. Mondal, and K. Thijssen, *Active particles knead three-dimensional gels into porous structures*, Phys. Rev. Lett. **133**, 228301 (2024).

[70] D. Grober, I. Palaia, M. C. Uçar, E. Hannezo, A. Šarić, and J. Palacci, *Unconventional colloidal aggregation in chiral bacterial baths*, Nat. Phys. **19**, 1680 (2023).

[71] M. S. Peterson, A. Baskaran, and M. F. Hagan, *Vesicle shape transformations driven by confined active filaments*, Nat. Commun. **12**, 7247 (2021).

[72] K. R. Prathyusha, F. Ziebert, and R. Golestanian, *Emergent conformational properties of end-tailored transversely propelling polymers*, Soft Matter **18**, 2928 (2022).

[73] L. Theeyancheri, S. Chaki, T. Bhattacharjee, and R. Chakrabarti, *Migration of active rings in porous media*, Phys. Rev. E **106**, 014504 (2022).

[74] H. Wen, Y. Zhu, C. Peng, P. S. Kumar, and M. Laradji, *Collective motion of cells modeled as ring polymers*, Soft Matter **18**, 1228 (2022).

[75] Z. Mokhtari and A. Zippelius, *Dynamics of active filaments in porous media*, Phys. Rev. Lett. **123**, 028001 (2019).

[76] C. Kurzthaler, S. Mandal, T. Bhattacharjee, H. Löwen, S. S. Datta, and H. A. Stone, *A geometric criterion for the optimal spreading of active polymers in porous media*, Nat. Commun. **12**, 7088 (2021).

[77] L. Theeyancheri, S. Chaki, T. Bhattacharjee, and R. Chakrabarti, *Active dynamics of linear chains and rings in porous media*, J. Chem. Phys. **159**, 014902 (2023).

[78] J.-F. Boudet, J. Lintuvuori, C. Lacouture, T. Barois, A. Deblais, K. Xie, S. Cassagnere, B. Tregon, D. B. Brückner, J.-C. Baret *et al.*, *From collections of independent, mindless robots to flexible, mobile, and directional superstructures*, Sci. Rob. **6**, eabd0272 (2021).

[79] J. Veenstra, C. Scheibner, M. Brandenbourger, J. Binysh, A. Souslov, V. Vitelli, and C. Coulais, *Adaptive locomotion of active solids*, Nature (London) **639**, 935 (2025).